High-Temperature Corrosion of Unpassivated Carbon Steel in Simulated Boiler Water: Electrochemical Thresholds and Mechanisms for Chloride and Sulphate Contamination

Benjamin A. Loder‡ and William G. Cook**

‡Corresponding author. E-mail: bloder@unb.ca.

*Centre for Nuclear Energy Research (CNER) - University of New Brunswick, 2 Garland Court, Fredericton, New Brunswick, E3B 5A3, Canada

ABSTRACT

The presence of chloride (Cl^-) and sulphate (SO_4^{2-}) in boiler water poses a significant threat to carbon steel integrity, yet their specific corrosion mechanisms and interaction at industrially relevant high temperatures remain poorly characterized. This study quantifies the accelerated corrosion thresholds and elucidates the distinct mechanistic roles of these contaminants for unpassivated SA210-A1 carbon steel in simulated all-volatile treatment (AVT) boiler water at 310 °C and 10.3 MPa. In situ corrosion rates were determined via linear polarization resistance (LPR), complemented by thermochemical equilibrium modelling (FactSage™). Results demonstrate that the corrosion threshold for SO_4^{2-} is 1.5 to 3 times higher than for Cl^-, validating industry heuristics. Mechanistic analysis reveals that Cl^- primarily acts by acidifying the solution and increasing iron solubility, whereas SO_4^{2-} accelerates corrosion through hydrothermal reduction to hydrogen sulfide. Furthermore, the chemical form of which the contaminants were introduced critically influences their combined effect: ammonium salts exhibit a buffering interaction that raises the combined threshold, while mineral acids produce a synergistic effect that lowers it. These findings provide quantitative thresholds and mechanistic clarity that establish a foundational basis for improving water chemistry guidelines and models.

KEY WORDS: All-Volatile Treatment (AVT), Boiler Water Chemistry, Carbon Steel, Chloride-Induced Corrosion, High-Temperature Aqueous Corrosion, High Temperature Electrochemical Measurements, Linear Polarization Resistance (LPR), Sulphate Reduction, Thermochemistry Modelling

1 INTRODUCTION

Ionic species like chloride (Cl^-) and sulphate (SO_4^{2-}) are often found in boiler water as a result of leaks in condenser tubing or through the dissolution of ion exchange resins in the feedwater treatment plant [1], [2]. These species are considered contaminants due to their known effect of accelerating the corrosion of boiler materials, more specifically ferrous metals [2], and are of particular concern as they can acidify the boiler water in stagnant locations such as under deposits [3]. Most of the current literature [4], [5], [6], [7], [8], [9], [10], [11], [12] on the corrosion of boiler materials subjected to Cl^- and SO_4^{2-} contamination, describe work completed at temperatures below that of typical industrial operating conditions. While they provide some insight into the mechanisms of contaminant induced corrosion, it is common for boilers to operate above 300 °C, and few studies, particularly those using electrochemical techniques, have surpassed this temperature. In recognition of this, the International Association for the Properties of Water and Steam (IAPWS) has emphasized that a better understanding of the corrosion mechanisms for such ionic contaminants in steam raising systems is still needed to support/improve cycle chemistry operating practices [13]. The Electric Power Research Institute (EPRI) identified this topic as a research priority and funded this research to address the knowledge gap.

Of the available literature, some interesting behaviour has been reported on the competition between Cl^- and SO_4^{2-} when both are present in solution. Niu et al [4], [5] has shown that the addition of SO_4^{2-} to a simulated all-volatile treatment (AVT) boiler water solution containing Cl^- can act to suppress pitting on 13Cr stainless steel at 90 °C. This was attributed to the formation of low solubility salt films that re-passivate sites from Cl^- pitting. Additionally, James et al. [14] in an investigation of corrosion fatigue crack initiation on SA210-Al carbon steel subjected to contaminated boiler water at 275 °C, showed that the addition of SO_4^{2-} to Cl^- containing solution increased the number of required cyclic loads before cracking was induced. This limiting effect was shown to be consistent for both AVT and phosphate treatment boiler water chemistries. In each of the above studies, as is often the case, Cl^- and SO_4^{2-} were added to the solution as NaCl and Na_2SO_4.

This study aims to further investigate the mechanisms of Cl^- and SO_4^{2-} induced corrosion under conditions more representative of an operating boiler. To do so, the linear polarization resistance (LPR) method [15], [16], [17], [18], [19], [20] was employed to measure, in situ, the corrosion rates of unpassivated SA210-Al boiler tube steel subjected to simulated AVT boiler water under various levels of Cl^- and SO_4^{2-} contamination. It is recognized that unpassivated steel does not exist in real operation; however, to elucidate the separate and combined effects of Cl^- and SO_4^{2-} anions, unpassivated steel was used as a starting point. Experiments were completed at 310 °C using AVT solutions contaminated with Cl^- or SO_4^{2-} individually, as well as a combination of both species. Additionally, trials were conducted with contaminant ions in the form of ammonium salts (NH_4Cl and $(NH_4)_2SO_4$), and later mineral acids (HCl and H_2SO_4), to better represent the chemistry conditions that may be present under deposits. To help better describe the influence of Cl^- and SO_4^{2-} on the observed corrosion behaviour and to compliment the experimental tests, simulations were completed using the FactSage™ thermochemistry modelling package [21]. This work is part of a longer-term initiative to provide accelerated corrosion thresholds for ionic contamination to better inform power cycle chemistry guidelines.

2 EXPERIMENTAL

2.1 Flow-through Electrochemical Cell

The electrochemical cell used in this study is of the three-electrode type, consisting of a platinum foil counter electrode (CE), SA210-A1 carbon steel working electrode (WE), and a platinum wire pseudo-reference electrode (RE). The CE is constructed from a ring of 0.5 mm thick platinum foil welded to a platinum wire (0.5 mm diameter), while the RE is a coiled piece of 0.5 mm diameter platinum wire. The WE-CE pair is contained within a 316 – stainless steel (SS) MHM4 Conax Technologies compression seal fitting. The WE-CE Conax assembly also contains a thermocouple to measure temperature at the fluid end of the probe. An exploded view of the WE-CE Conax assembly is shown in **Figure 1**. The platinum wire portion of the CE that passes through the Conax fitting is insulated with PTFE heat shrink, while a small gap between the platinum foil and steel follower is maintained to prevent electrical contact at the fluid end. The steel electrode is isolated using a yttria stabilized zirconia (YSZ) ceramic sheath in combination with PTFE heat shrink. Similar to the WE-CE assembly, the RE is contained within a separate 316-SS MHC2 Conax fitting and uses PTFE heat shrink to electrically isolate the platinum wire. The complete electrochemical cell is assembled by adding both the RE and WE-CE Conax components to a Swagelok 316-SS cross fitting, which serves as the body of the cell.

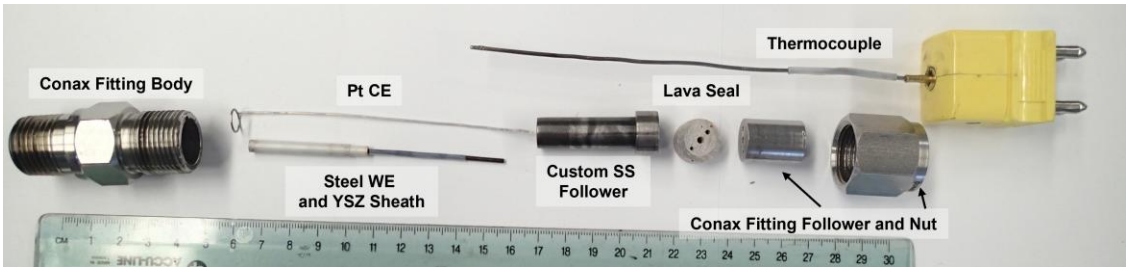

Figure 1. Exploded view of the WE-CE Conax assembly.

A once-through autoclave system (**Figure 2**) was used to facilitate testing within the electrochemical cell. Two 50 L Nalgene carboys provide separate storage of the uncontaminated and contaminated simulated AVT boiler water. Both carboys were continuously purged with argon gas to maintain a dissolved oxygen concentration below 10 µg/kg. Two parallel high performance liquid chromatography (HPLC) pumps (Eldex model 1HM) take fluid from each carboy. The flowrate of each pump was individually adjusted (0.01 mL/min resolution) depending on the desired contaminant concentration to achieve a target total flow rate of 5.00 mL/min. All tests were conducted at 310 °C and 10.3 MPa. Concentrations of the ionic contaminant species were determined from grab samples of the test rig effluent using a Dionex ICS-3000 Ion chromatography (IC) system.

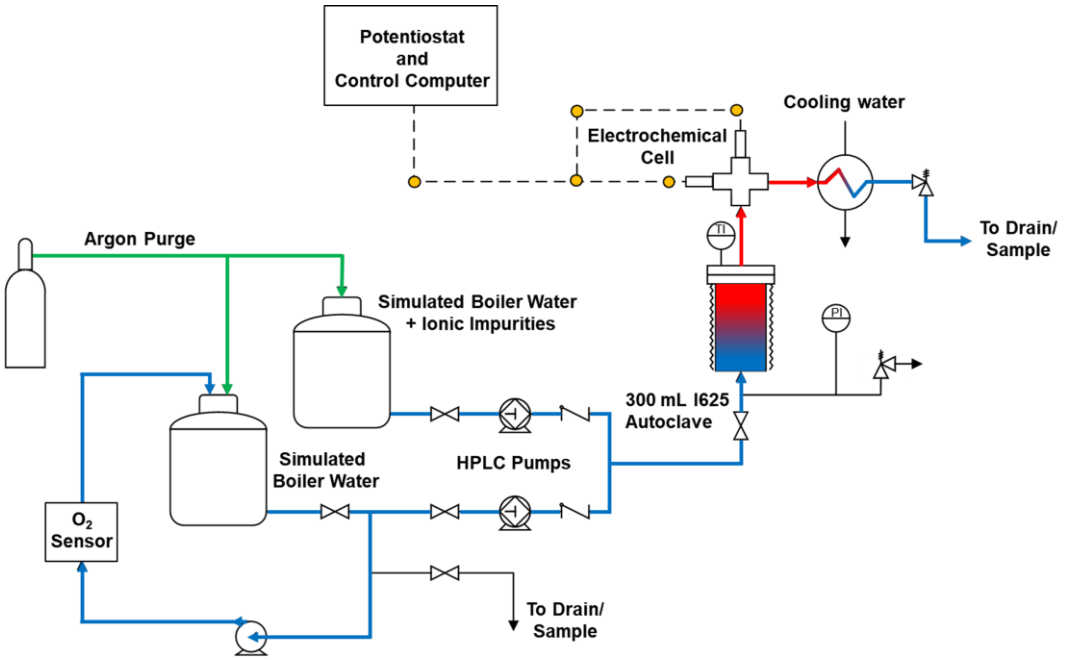

Figure 2. Simplified schematic diagram of the once-through autoclave test system.

2.2 Steel Electrodes

Boiler tube steel samples were prepared from SA210-A1 carbon steel with a composition (% w/w) of C 0.134%, Si 0.186%, Mn 0.683%, P 0.009%, S 0.004%, Cr 0.133%, Mo 0.038%, Ni 0.103%, Cu 0.143%, V 0.0025, balance Fe, machined into 90 mm long cylinders with two sections of different radii (1.5 mm and 0.88 mm). The cross-sectional surface at the tip of the larger end of the cylinder was exposed to the test solution during experiments, while the non-exposed end connects to the electrical leads of the potentiostat. The edge at the transition between radii is seated against a matching edge within the custom YSZ insert / Conax follower to secure the electrode in place, preventing ejection from the fitting once pressurized. Before each experimental trial, the steel electrodes were mechanically polished to 1200 grit and rinsed with deionized water and ethanol to remove any oils or debris.

2.3 Preparation of Test Solutions

Simulated boiler water was prepared by initially filling the two 50 L Nalgene reservoirs with 15 MΩ-cm deionized water. Each reservoir was then recirculated through mixed bed ion-exchange resin (Purolite UCW3700) for ~24 hours while sparging with argon gas to remove any trace impurities as well as any carbonate up-take while transferring the water.

Once purified, the pH was adjusted to 9.4 ± 0.05 at 25 °C by the injection of stock solutions of NH_4OH prepared by dilution from a standard solution of NH_4OH (28% w/w NH_3 basis, ACS reagent, Sigma-Aldrich). The Cl^- and SO_4^{2-} impurities were added to the contaminant reservoir as stock solutions of either NH_4Cl and $(NH_4)_2SO_4$ or HCl and H_2SO_4. Ammonium chloride and ammonium sulfate stock solutions were prepared gravimetrically from NH_4Cl (≥99.5%, ACS Reagent, Sigma-Aldrich) and $(NH_4)_2SO_4$ (≥99.0%, Sigma-Aldrich); while the mineral acid contaminant solutions were prepared by dilution from standard solutions of HCl (36.5% w/w, Certified ACS Plus, Fisher Chemical) and H_2SO_4 (95.0% w/w, Certified ACS Plus, Fisher Chemical). Grab samples of each test solution were taken to verify the pH and conductivity using a Fisherbrand Accumet XL500 benchtop pH/conductivity meter.

2.4 Accelerated Corrosion Threshold Testing

During each trial, the contaminant concentration in the test solution supplied to the electrochemical was increased stepwise until the maximum concentration contained in the contaminated simulated boiler water carboy was reached. For each incremental step, the electrochemical cell was allowed to stabilize for approximately 12 hours prior to the collection of electrochemical data and collection of grab samples from the test rig effluent.

The corrosion rate of the steel electrode was monitored through the collection of LPR measurements. Prior to a LPR measurement, the open circuit potential (OCP) was monitored for 60 seconds to check for stability within approximately +/- 5 mV. This was done to ensure consistent results, since drift in the measured electrochemical corrosion potential can complicate the collection of linear polarization data. To help overcome this, a relatively wide potential range of ± 50 mV was applied to the steel electrode during an LPR measurement to ensure that the scan crossed the zero current potential, as this is a requirement for the determination of polarization resistance. However, as is typical for this technique, only data within ± 10 mV of the zero current potential was used to determine the polarization resistance. The electrochemical measurements were performed using a Princeton Applied Research Versastat 3 potentiostat.

When analysing the LPR data, the overall magnitude of the corrosion rates varied between each trial. Differences in the tolerance between the steel electrodes and the surrounding YSZ ceramic sheath resulted in gaps between the materials and because of this, the exposed surface area of the electrode was likely different between trials resulting in the observed discrepancies. While it was originally intended that this area would be isolated to the cross-section at the tip of the electrode, the varying tolerances made this unfeasible. Since the exact electrode surface area for each trial is unknown, it is more useful to to interpret the general trends on a relative corrosion rate scale to correct for these differences. To place the results on such a basis, each data point is adjusted based on the initial uncontaminated corrosion rate for the respective trial.

For each trial, the accelerated corrosion threshold was identified as the point at which either of the following two criteria were met: (i) in cases where the corrosion rate was observed to gradually decrease over the initial concentration step changes, the accelerated corrosion threshold was interpreted as the point at which a sustained change in the overall direction of the corrosion rate trend occurred, i.e., decreasing trend transitioning to a continually increasing trend, or; (ii) when the corrosion rate remained relatively stable over the initial concentration step changes,

the accelerated corrosion threshold was taken as the concentration where a net increase of ≥ 5 % occurred, provided that the corrosion rate continued to climb as contaminant concentrations were further increased.

3 RESULTS AND DISCUSSION

Both individual and combined contaminant trials were completed under AVT chemistry on unpassivated steel electrodes, with this series of trials first carried out using ammonium salts, then repeated by adding the contaminants as mineral acids. Originally, the intent was to only complete trials using the ammonium salt form of the contaminants to match the composition of the uncontaminated AVT test solution. Since NH_4^+ is already present in AVT solution, this form of contamination would not introduce additional cations like Na^+. However, after completing the initial series of experiments this approach was revaluated given that, in an actual boiler, ionic contaminants accumulate under deposits resulting in relatively acidic localized chemistry [3]. Since the present experimental methodology did not include initial passive oxides or deposits on the steel samples, the addition of Cl^- and SO_4^{2-} contaminants in mineral acid form was thought to better represent these conditions. In this approach, the pH of the test solution corresponds more directly to the contaminant concentration, therefore it is a closer representation of the system beneath a deposit layer without the need for actually having the deposit present. The resulting relative corrosion rate trends are shown in **Figure 3** and **Figure 4** for tests completed with ammonium salts and mineral acids respectively. A summary of the accelerated corrosion thresholds observed for each trial are listed in **Table 1**.

Comparing the corrosion rate trends measured for the individual contaminants, the accelerated corrosion threshold for SO_4^{2-} is 1.5 – 3x higher than for Cl^-, with the acid and ammonia salt contaminants representing the lower and upper ends of this range respectively. The typical assumption used within the thermal power generation industry is that Cl^- is approximately twice as corrosive as SO_4^{2-}, therefore, concentration limits for SO_4^{2-} are often listed as simply 2x the maximum allowable Cl^- specification. This heuristic appears to be relatively consistent with the experimental results shown here. The accelerated corrosion thresholds for individual Cl^- contamination also show reasonable agreement to a value of approximately 200 µg/kg reported by Xiong et al. [9], derived from weight loss measurements on carbon steel exposed to static autoclave testing at 300 °C. The results from the combined contaminant trials showed that when the contaminants are added as ammonium salts, the accelerated corrosion threshold for the combined Cl^- and SO_4^{2-} is closer to the threshold for individual SO_4^{2-} contamination. In contrast to this, when added as mineral acids, the accelerated corrosion threshold aligns closer to that for individual Cl^-.

To help investigate these differences, the FactSage™ Equilib thermochemistry modelling package [21] was used to simulate the iron-water system when exposed to the various types of Cl^- and SO_4^{2-} contamination used in the experimental trials. For each contaminant type, the contaminant concentration from the trials along with an ammonia concentration of 1 mg/kg (corresponding to a $pH_{25\,°C}$ of ~ 9.4) and a dissolved O_2 concentration of 10 µg/kg were used as model inputs. For combined Cl^- and SO_4^{2-} contamination, simulations were completed at several $[SO_4^{2-}]$ to $[Cl^-]$ ratios. In all simulations, an excess of solid iron was assumed to be in contact with the solution to mimic the presence of the initially unpassivated carbon steel electrode. This was chosen to maintain iron in solution at its solubility limit corresponding to the given solution chemistry to represent conditions at the electrode/solution interface. Using this approach, the pH_T values and total iron solubilities at 310 °C were calculated for each trial, the results of which are shown in **Figure 5** and **Figure 6** for the ammonium salt tests while the mineral acid tests are shown in **Figure 7** and **Figure 8**.

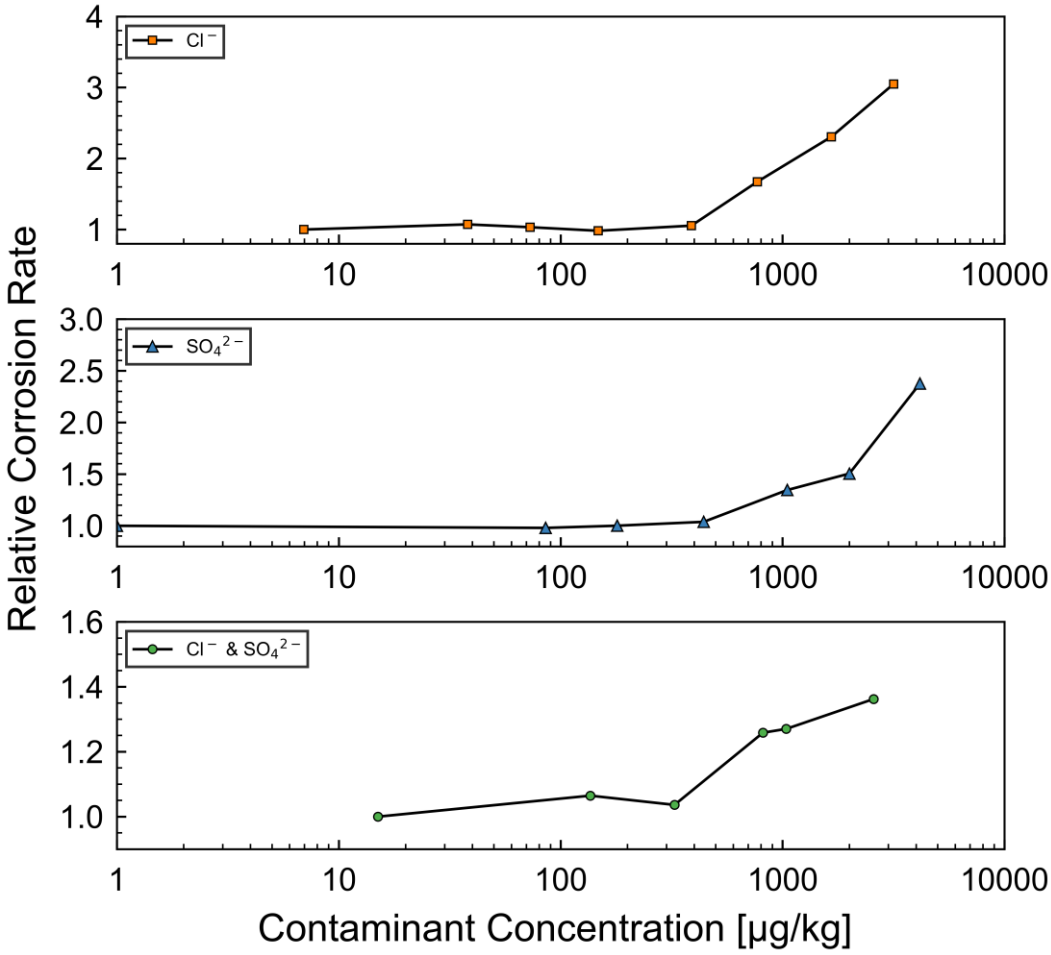

Figure 3. Relative corrosion rates trends from LPR measurements taken on initially unpassivated steel exposed to ammonium salt contaminants. Note that for the combined Cl^- & SO_4^{2-} trial [Cl^-] is shown, while [SO_4^{2-}] = 1.7 x [Cl^-].

Table 1. Summary of the threshold contaminant concentrations for accelerated corrosion.

Contaminant Type	Species	LPR Corrosion Threshold in (µg/kg): Cl^- / SO_4^{2-}
Ammonium Salts	Cl^-	150 – 390
	SO_4^{2-}	440 – 1050
	Cl^- & SO_4^{2-}	330 – 820 / 560 – 1400
Mineral Acids	Cl^-	240 – 470
	SO_4^{2-}	320 – 670
	Cl^- & SO_4^{2-}	200 – 530 / 300 – 870

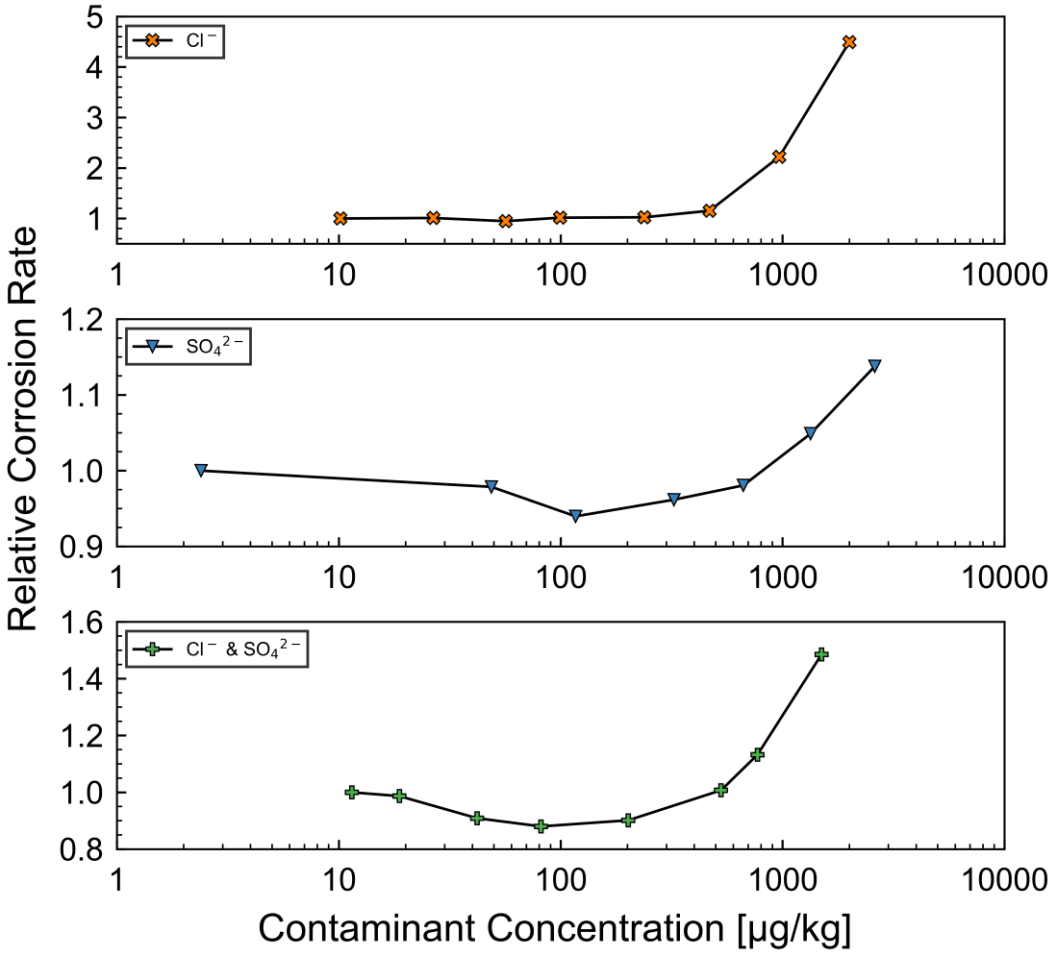

Figure 4. Relative corrosion rates trends from LPR measurements taken on initially unpassivated steel exposed to acidic contaminants. Note that for the combined Cl^- & SO_4^{2-} trial $[Cl^-]$ is shown, while $[SO_4^{2-}] = 1.5 \times [Cl^-]$.

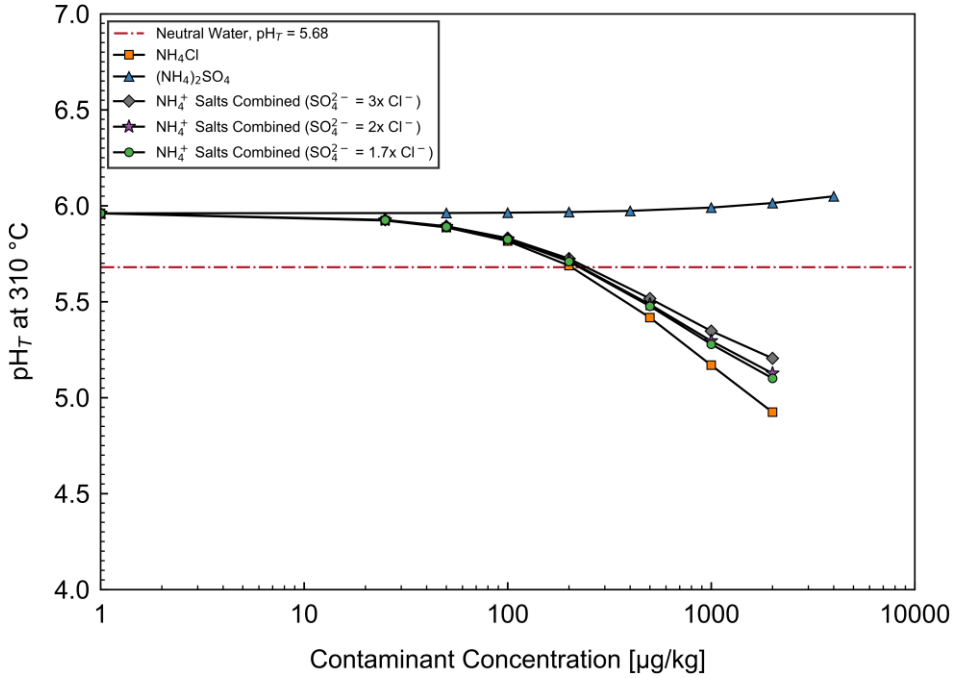

Figure 5. Calculated pH_T for ammonium salt contaminants. Note that for combined contaminants the solubilities are plotted against the Cl^- concentration.

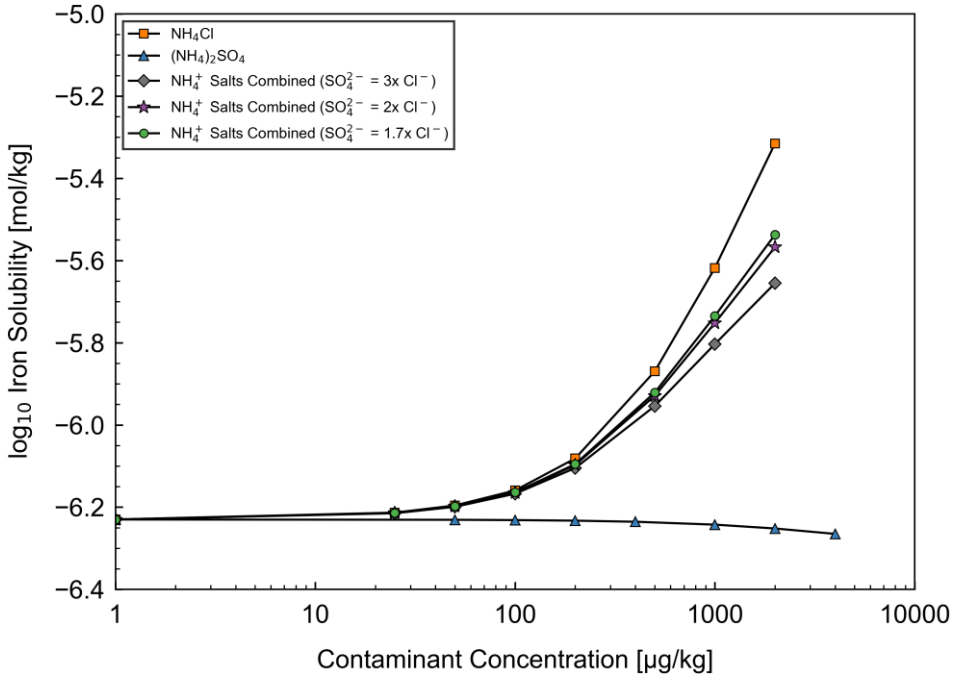

Figure 6. Calculated total iron solubilities at 310 °C for ammonium salt contaminants. Note that for combined contaminants the solubilities are plotted against the Cl^- concentration.

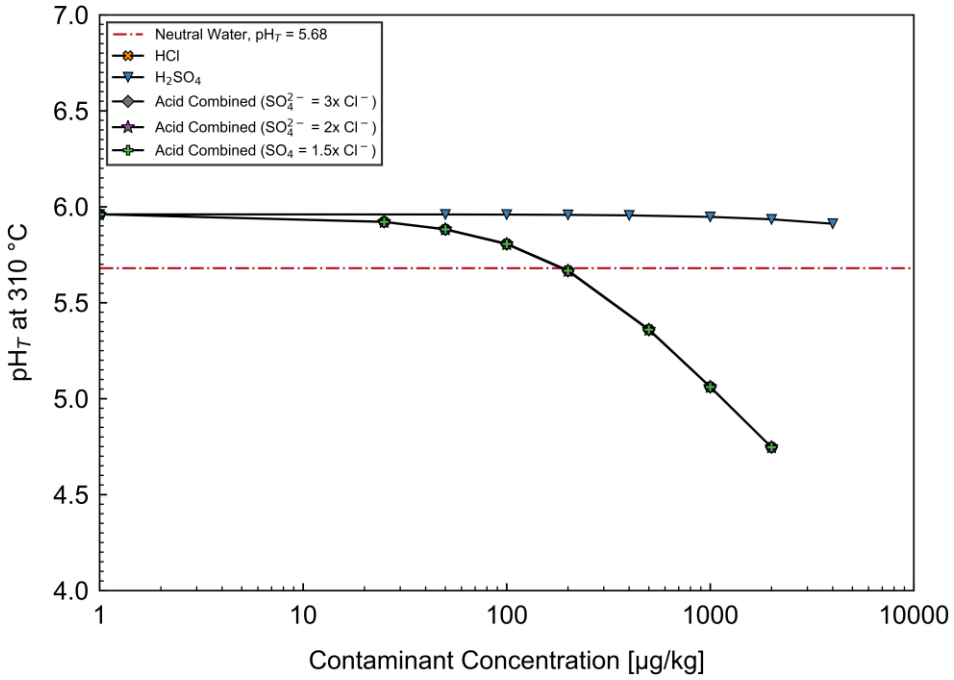

Figure 7. Calculated pH_T for acidic contaminants. Note that for combined contaminants the solubilities are plotted against the Cl^- concentration.

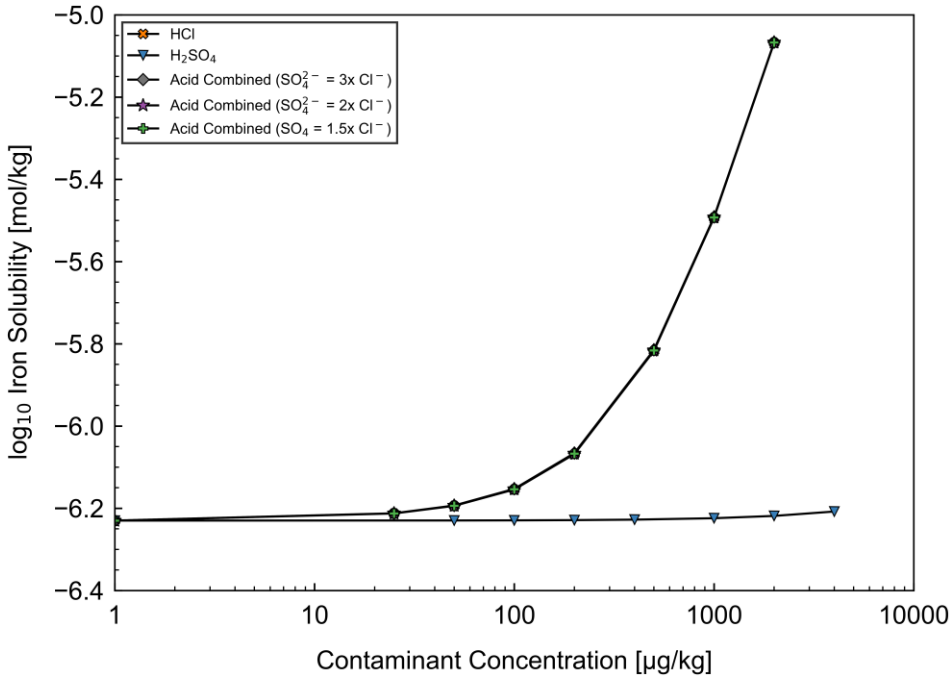

Figure 8. Calculated total iron solubilities at 310 °C for acidic contaminants. Note that for combined contaminants the solubilities are plotted against the Cl^- concentration.

3.1 Chloride Corrosion Behaviour

The rates of iron/magnetite dissolution and precipitation are governed by their solubility [22], where the concentration gradient between the surface of the steel/oxide film and the bulk solution is a major driving force behind the rate of both processes. Therefore, with increased solubility, it can be expected that the rate of iron dissolution will follow. As shown from the equilibrium modeling results in **Figure 6** and **Figure 8**, the Cl^- contamination very clearly increases the solubility of iron. This holds true whether it is first introduced as NH_4Cl or HCl. The underlying cause of this increase is suspected to be a result of several factors. First, at elevated temperatures, either of the two Cl^- containing species will acidify the solution as shown by the calculated pH_T trends in **Figure 5** and **Figure 7**. Since the pH of uncontaminated AVT boiler water is only slightly alkaline at 310 °C, decreasing the pH will increase the solubility of iron/magnetite as experimentally demonstrated in various other studies [23], [24], [25].

Second, it is well known that Cl^- solutions will form highly soluble complexes with iron. The formation of which prevents the complexed iron from reprecipitating as magnetite at the surface of the steel by carrying it away in the bulk solution [26]. When Cl^- is present at a high enough concentration, this complex formation is likely to have an effect on the total amount of dissolved iron. This was supported by the FactSage™ simulations, which showed that the formation of $FeCl^+$ became increasingly favourable beyond a Cl^- concentration of 200 µg/kg (approximately the experimentally measured accelerated corrosion threshold) for both forms of contamination. This is shown for the ammonium salt and mineral acid trials in **Figure 9** and **Figure 10** respectively. However, compared to the impact of pH_T, the increase in dissolved iron due to the formation of $FeCl^+$ only constitutes a fraction of the overall iron solubility.

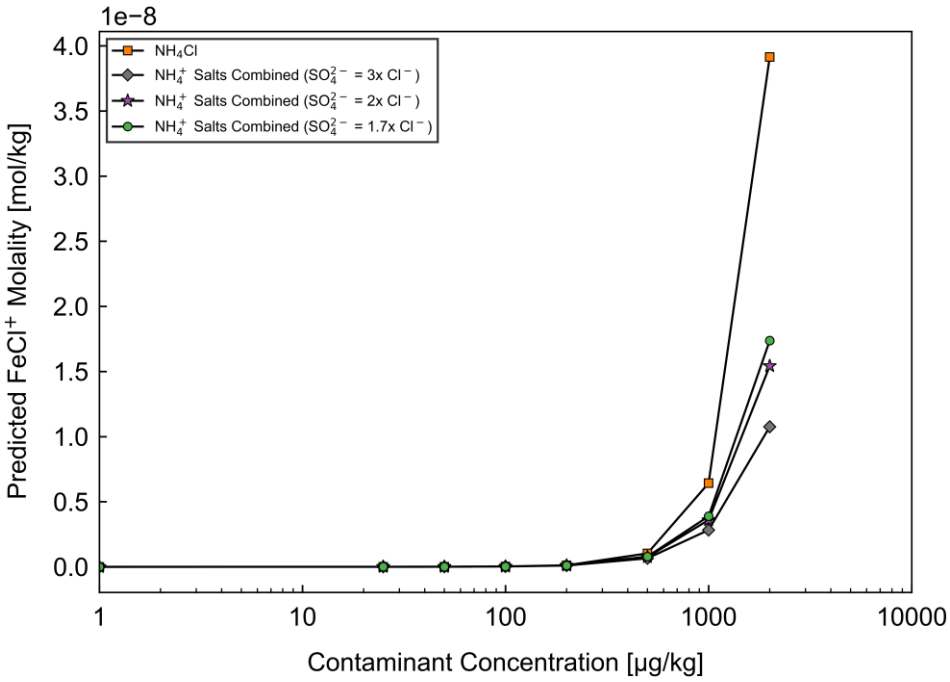

Figure 9. FactSage™ predicted $FeCl^+$ molality at 310 °C for ammonium salt contaminants. Note that for combined contaminants the solubilities are plotted against the Cl^- concentration.

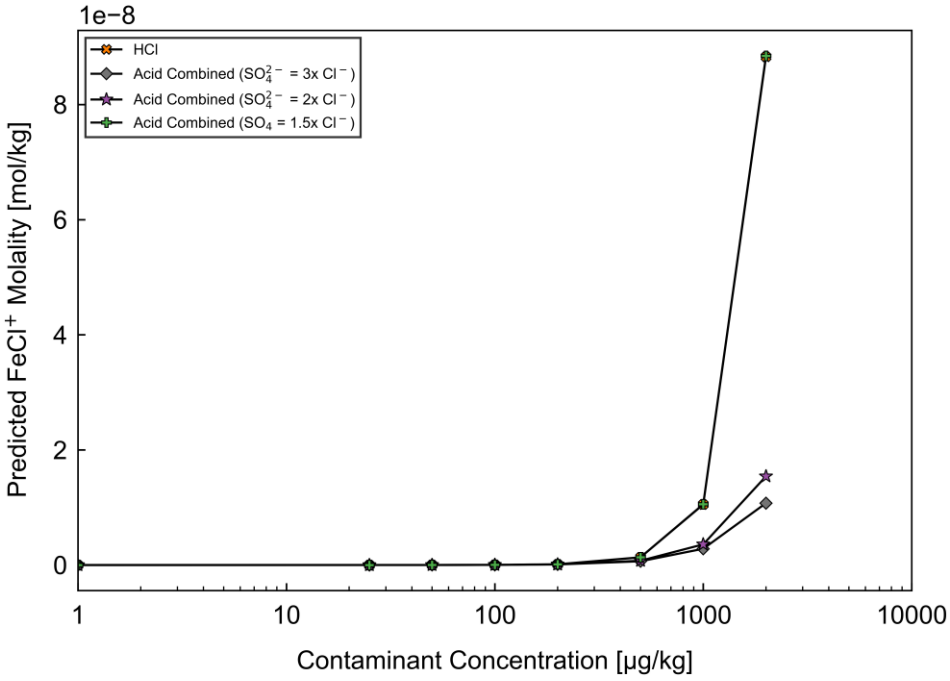

Figure 10. FactSage™ predicted $FeCl^+$ molality at 310 °C for acidic contaminants. Note that for combined contaminants the solubilities are plotted against the Cl^- concentration.

Additionally, the outermost surface of an oxide film in contact with an aqueous solution is covered with a layer of hydroxyl groups. In acidic solutions, these hydroxyl groups interact with protons to form a positive surface charge [27], [28], [29]. The adsorption of Cl^- due to coulombic attraction will act to depolarize the surface allowing protons to more readily participate in hydrogen reduction as they are no longer repelled by the positive charge [27], [28], [30]. As a result, iron dissolution is accelerated. While the steel electrode lacks a protective oxide film at the beginning of each trial, upon exposure to the high temperature solution the surface will quickly begin to passivate. Each of the factors

discussed above will affect the rate at which this passivation process can proceed. Therefore, the accelerated corrosion threshold can then be said to represent the point at which the rate of the Cl^- assisted iron/magnetite dissolution dominates over the rate of passivation. Additionally, as demonstrated by Zhang et al. [31], the incorporation of Cl^- into the barrier layer of magnetite as it grows on the steel's surface, can potentially negate the protection it would normally provide.

3.2 Sulphate Corrosion Behaviour

It is clear from **Figure 5** through **Figure 8** that whether added in ammonium salt or mineral acid form, SO_4^{2-} has a negligible effect on the pH_T and by extension the solubility of iron, at least within the tested concentration range. In fact, when added as $(NH_4)_2SO_4$ the calculated iron solubility decreases slightly as the SO_4^{2-} concentration is increased, with this being a result of the pH_T shifting to slightly more alkaline values. This suggests that the impact of individual SO_4^{2-} contamination on the dissolution of the carbon steel must primarily be a result of charge transfer between the contaminant and the steel. Under hydrothermal conditions it has been demonstrated that SO_4^{2-} is reduced to H_2S by coupling with the oxidation of dissolved H_2 as described by Equation (1) [32]. The simulations completed in FactSage™ also showed that this reduction is predicted whether the SO_4^{2-} is added as $(NH_4)_2SO_4$ or H_2SO_4.

$$4\,H_{2\,(g)} + SO_{4\,(aq)}^{2-} + 2\,H_{(aq)}^{+} \rightleftharpoons H_2S_{(g)} + 4\,H_2O_{(l)} \qquad (1)$$

In the presence of carbon steel, it is hypothesized that the reduction of SO_4^{2-} could at least partially couple with the dissolution of iron as a source of electrons through the following half-cell reaction:

$$SO_{4\,(aq)}^{2-} + 10\,H_{(aq)}^{+} + 8\,e^- \rightleftharpoons H_2S_{(g)} + 4\,H_2O_{(l)} \qquad (2)$$

Since SO_4^{2-} reduction will occur without the presence of iron [32], it is likely that the reaction represented by Equation (1) is the dominant pathway, and it is only at relatively high concentrations that the amount reduced through Equation (2) has any appreciable impact on iron dissolution. From this it would be expected that the accelerated corrosion threshold for individual SO_4^{2-} contamination should be higher than for Cl^-, with this being supported by the results of the experimental trials. The increasing pH_T shown for additions of $(NH_4)_2SO_4$ in **Figure 5** can also be explained by the consumption of H^+ when SO_4^{2-} is reduced to H_2S. Unlike H_2SO_4, which directly adds H^+ to the system, the dissociation of $(NH_4)_2SO_4$ contributes to an equilibrium between NH_4^+ and NH_3. Although this equilibrium is highly shifted towards NH_3 at elevated temperatures [3], [33], [34], [35], [36], fewer protons are released than for H_2SO_4, and the overall effect of the SO_4^{2-} reduction results in a slight loss of H^+.

3.3 Combined Chloride and Sulphate Corrosion Behaviour

When Cl^- and SO_4^{2-} are combined, the impact of contamination on the corrosion of the carbon steel is more complex. This is particularly evident, as the form in which the contaminant species are introduced appears to influence their overall behaviour. When added as HCl and H_2SO_4 there is no distinct difference in the pH_T and therefore the iron solubility (**Figure 7** and **Figure 8**) between a combination of Cl^- and SO_4^{2-} or Cl^- alone. This was found to be consistent even when the ratio between the two species was adjusted in the FactSage™ simulations.

In contrast to this, when compared to individual NH_4Cl contamination, the addition of $(NH_4)_2SO_4$ reduces the overall impact of the mixture on the pH_T and therefore the iron solubility (**Figure 5** and **Figure 6**). Interestingly, the simulations showed that increasing the ratio of SO_4^{2-} to Cl^- further dampens any change. As shown previously in **Table 1**, the accelerated corrosion threshold of the combined contaminants was higher than for either individual species. This suggests that when added as ammonium salts, SO_4^{2-} will suppress the corrosive behaviour of Cl^-.

Despite numerous studies [4], [5], [14], [26], [37], [38], [39], [40], [41], [42] reporting similar limiting effects of the SO_4^{2-} ion on the corrosion of steels in Cl^- solutions, the exact cause has remained speculative. Unfortunately, no post exposure surface analysis of the steel electrodes was completed in this present study. Therefore, it is unknown whether the formation of protective iron SO_4^{2-} salt films like those reported elsewhere [4], [5], [37], [40], [42] had occurred. In addition, the concentration of contaminants in these studies were reported to be on the order of 100 mg/kg up to several parts per thousand (g/kg), which is far higher than typical for boiler water even under contaminant excursion conditions. It is also unknown if the precipitation of these species would be favourable at 310 °C, as most other works have been completed below 100 °C. Notably, no such species were predicted by the simulations performed in FactSage™.

Based on the analysis of the individual contaminant trials, it is more likely that the reduction of SO_4^{2-} when added as $(NH_4)_2SO_4$ slightly buffers the acidity of the Cl^-. Since the effect of Cl^- contamination on the corrosion behaviour of initially unpassivated steel appears to be primarily a factor of increasing the solubility of iron through lowering the pH, the addition of $(NH_4)_2SO_4$ acts to delay the accelerated corrosion threshold. When added as HCl and H_2SO_4, although the reduction of SO_4^{2-} reduces the effective acidity of the H_2SO_4, there is still a net gain of protons. Therefore, the accelerated corrosion threshold of the combined contaminants is slightly lower than that for the individual HCl contamination.

3.4 Practical Considerations

As previously noted, in real operation, unpassivated or bare steel boiler tube surfaces do not occur. Accordingly, the accelerated corrosion threshold concentrations presented in **Table 1** are most valuable for (i) advancing the understanding of Cl^- and SO_4^{2-} corrosion behaviour at high temperature, and (ii) demonstrating the capabilities of the high-temperature electrochemical cell. They should not, however, be interpreted as shutdown limits for boiler water. This distinction arises due to two factors:

(i) Real boiler tube surfaces are protected by a magnetite layer; thus, the contaminant concentrations required to induce accelerated corrosion (i.e., passive film breakdown) are expected to be significantly higher than the values reported in **Table 1**.

(ii) Boiler water shutdown limits are based on ionic contamination in the boiler drum blowdown stream. Due to their low volatility and solubility in the steam phase, species like Cl^- and SO_4^{2-} concentrate beneath deposits subjected to a high heat flux, producing local environments with orders of magnitude higher contaminant concentrations than those measured in bulk boiler water. Evaluating shutdown limits therefore requires accounting for this concentrating effect at the passivated boiler tube surface.

It was also observed that when added as ammonium salts, SO_4^{2-} buffered the acidification of the test solution from Cl^-, producing a higher accelerated corrosion threshold concentration for combined NH_4Cl and $(NH_4)_2SO_4$ relative to NH_4Cl alone. It is unlikely, however, that NH_4Cl or $(NH_4)_2SO_4$ would form or be present in a boiler. Although ammonium salts were originally selected to avoid introducing additional cations into the AVT test solutions, these results indicate that their use can create unique high-temperature chemistry not representative of boiler operation. For future studies, mineral acids should be preferred as contaminant sources over both ammonium and sodium salts, as they more accurately simulate localized chemistry beneath boiler tube deposits. This consideration is particularly important if synthetic deposits and high heat flux exposure cannot be combined with electrochemical measurement techniques.

4 CONCLUSIONS

- The accelerated corrosion threshold for individual SO_4^{2-} contamination on unpassivated carbon steel in 310 °C simulated AVT boiler water was found to be 1.5 – 3x higher (depending on the initial form of the contamination) than for individual Cl^-, supporting the current industry heuristic that Cl^- is approximately twice as corrosive as SO_4^{2-}.

- The impact of Cl^- on the corrosion behavior of unpassivated carbon steel in the simulated AVT boiler water is primarily a factor of its ability to acidify the solution and therefore increase the solubility of iron.

- The impact of SO_4^{2-} on the dissolution of the unpassivated carbon steel is suspected to be a result of charge transfer between the contaminant and the steel, rather than direct changes to the solution chemistry. It is proposed that the reduction of the SO_4^{2-} anion to H_2S under hydrothermal conditions may provide an additional cathodic reaction to accelerate iron dissolution once contaminant concentrations are sufficiently high.

- When Cl^- and SO_4^{2-} are both present in 310 °C simulated AVT boiler water, the combined impact on the accelerated corrosion threshold varies based on the initial form of the contaminants. When added as ammonium salts, SO_4^{2-} acts to buffer the acidification of the solution by Cl^-, partially mitigating its effect on the solubility of iron. As a result, the accelerated corrosion threshold for the combined contaminants is higher than for individual Cl^-. This buffering effect is negligible when the contaminants are added as HCl and H_2SO_4, resulting in a lower accelerated corrosion threshold than for solutions contaminated with HCl alone. However, since ammonium salts are unlikely to form under boiler conditions, mineral acids represent the more relevant contaminant form and should be used for future studies.

5 ACKNOWLEDGEMENTS

The Electric Power Research Institute (EPRI), the International Association for the Properties of Water and Steam (IAPWS), and David Addison at Thermal Chemistry Ltd. are gratefully acknowledged for their financial support and collaboration with this work. The authors also acknowledge the contributions of the following individuals: Adon Briggs, for his extensive work in manufacturing the custom fittings and electrodes used throughout the study; Dr. Lihui Liu for her assistance with the ion chromatography analyses; and Brad McCann and Chester Morris, for their support in modifying and maintaining the test apparatus. Finally, the authors extend their gratitude to Siemens Heat Transfer Technology for providing a section of boiler tube from which the steel electrodes were machined.

6 REFERENCES

1. D. J. Flynn Ed. and Nalco Water, *The Nalco water handbook*, Fourth edition. New York: McGraw-Hill Education, 2018.
2. International Association for the Properties of Water and Steam, “Technical Guidance Document: Volatile treatments for the steam-water circuits of fossil and combined cycle/HRSG power plants.” 2015.
3. P. Cohen Ed. and the ASME Research and Technology Committee on Water and Steam in Thermal Power Systems, *The ASME handbook on water technology for thermal power systems*, New York, NY: American Society of Mechanical Engineers, 1989.
4. L.-B. Niu and K. Nakada, “Effect of chloride and sulfate ions in simulated boiler water on pitting corrosion behavior of 13Cr steel,” *Corrosion Science*, vol. 96, pp. 171–177, Jul. 2015, doi: 10.1016/j.corsci.2015.04.005.

5. L.-B. Niu, K. Okano, S. Izumi, K. Shiokawa, M. Yamashita, and Y. Sakai, “Effect of chloride and sulfate ions on crevice corrosion behavior of low-pressure steam turbine materials,” *Corrosion Science*, vol. 132, pp. 284–292, Mar. 2018, doi: 10.1016/j.corsci.2017.12.017.
6. D. Iravani and R. Arefinia, “Effectiveness of one-to-one phosphate to chloride molar ratio at different chloride and hydroxide concentrations for corrosion inhibition of carbon steel,” *Construction and Building Materials*, vol. 233, p. 117200, Feb. 2020, doi: 10.1016/j.conbuildmat.2019.117200.
7. Z. Zhu, X. Jiao, X. Tang, and H. Lu, “Effects of SO_4^{2-} concentration on corrosion behaviour of carbon steels,” *Anti-Corrosion Methods and Materials*, vol. 62, no. 5, pp. 322–326, 2015, doi: 10.1108/ACMM-01-2014-1342.
8. L.-B. Niu, H. Kato, K. Shiokawa, K. Nakamura, M. Yamashita, and Y. Sakai, “Electrochemical Crevice Corrosion Behaviors of Low-Pressure Steam Turbine Materials in the Simulated Boiler Water Added Chloride and Sulfate Ions,” *Materials Transactions*, vol. 54, no. 12, pp. 2225–2232, 2013, doi: 10.2320/matertrans.M2013202.
9. S. Xiong, Z. Zhu, and L. Jing, “Influence of Cl^- ions on the pitting corrosion of boiler water-wall tube and its principle,” *Anti-Corrosion Methods and Materials*, vol. 59, no. 1, pp. 3–9, Jan. 2012, doi: 10.1108/00035591211190481.
10. X. Wu, S. Huang, W. Zhang, Q. Feng, and Y. Huang, “Study on the electrochemical corrosion behavior of industrial boilers,” *AIP Conference Proceedings*, vol. 1971, no. 1, p. 020024, Jun. 2018, doi: 10.1063/1.5041119.
11. B. O. Hasan and S. A. Sadek, “The effect of temperature and hydrodynamics on carbon steel corrosion and its inhibition in oxygenated acid–salt solution,” *Journal of Industrial and Engineering Chemistry*, vol. 20, no. 1, pp. 297–307, Jan. 2014, doi: 10.1016/j.jiec.2013.03.034.
12. J. Macak, P. Sajdl, P. Kucera, and R. Novotny, In-situ study of high temperature aqueous corrosion by electrochemical techniques, *NACE Corrosion-2005*, Houston, Texas, 2005.
13. International Association for the Properties of Water and Steam, “Certified Research Need – ICRN#25: Corrosion mechanisms related to the presence of contaminants in steam/water circuits, particularly in boiler water.” Jun. 2014.
14. B. A. James, L. D. Paul, and M. T. Miglin, “Low cycle fatigue crack initiation in SA-210 A1 carbon steel boiler tubing in contaminated boiler water,” in *American Society of Mechanical Engineers, Pressure Vessels and Piping Division PVP*, 1990, pp. 13–19.
15. E. J. Simmons, “Use of the Pearson Bridge in Corrosion Inhibitor Evaluation,” *Corrosion*, vol. 11, no. 6, pp. 25–30, Jun. 1955, doi: 10.5006/0010-9312-11.6.25.
16. R. V. Skold and T. E. Larson, “Measurement of the instantaneous corrosion rate by means of polarization data,” *Corrosion*, vol. 13, no. 2, pp. 69–72, 1957.
17. M. Stern and A. L. Geary, “Electrochemical Polarization: I. A Theoretical Analysis of the Shape of Polarization Curves,” *Journal of The Electrochemical Society*, p. 9, 1957, doi: 10.1149/1.2428496
18. M. Stern, “Electrochemical polarization: II. ferrous-ferric electrode kinetics on stainless steel,” *Journal of The Electrochemical Society*, vol. 104, no. 9, p. 559, 1957, doi: 10.1149/1.2428653
19. M. Stern, “Electrochemical Polarization: III. Further Aspects of the Shape of Polarization Curves,” *Journal of The Electrochemical Society*, 1957, doi: 10.1149/1.2428438
20. M. Stern, “A Method for Determining Corrosion Rates from Linear Polarization Data,” *Corrosion*, vol. 14, no. 9, pp. 60–64, Sep. 1958, doi: 10.5006/0010-9312-14.9.60.
21. C. W. Bale et al., “FactSage thermochemical software and databases, 2010–2016,” *Calphad*, vol. 54, pp. 35–53, Sep. 2016, doi: 10.1016/j.calphad.2016.05.002.
22. W. G. Cook, “Experiments and Models of General Corrosion and Flow-Assisted Corrosion of Materials in Nuclear Reactor Environments,” *University of New Brunswick*, Fredericton, N.B., 2005.

23. F. H. Sweeton and C. F. Baes, “The solubility of magnetite and hydrolysis of ferrous ion in aqueous solutions at elevated temperatures,” *The Journal of Chemical Thermodynamics*, vol. 2, no. 4, pp. 479–500, 1970, doi: 10.1016/0021-9614(70)90098-4
24. P. R. Tremaine and J. C. LeBlanc, “The solubility of magnetite and the hydrolysis and oxidation of Fe2+ in water to 300°C,” *Journal of Solution Chemistry*, vol. 9, no. 6, pp. 415–442, Jun. 1980, doi: 10.1007/BF00645517.
25. S. E. Ziemniak, M. E. Jones, and K. E. S. Combs, “Magnetite solubility and phase stability in alkaline media at elevated temperatures,” *Journal of Solution Chemistry*, vol. 24, no. 9, pp. 837–877, 1995, doi: 10.1007/BF00973442
26. S. E. Traubenberg and R. T. Foley, “The Influence of Chloride and Sulfate Ions on the Corrosion of Iron in Sulfuric Acid,” *Journal of The Electrochemical Society*, vol. 118, no. 7, p. 1066, 1971, doi: 10.1149/1.2408248.
27. [E. McCafferty, *Introduction to corrosion science*, Springer Publishing 2010., doi: 10.1007/978-1-4419-0455-3.
28. R. M. Cornell, A. M. Posner, and J. P. Quirk, “Kinetics and Mechanisms of the Acid Dissolution of Goethite (a-FeOOH),” *Journal of Inorganic and Nuclear Chemistry*, vol. 38, no. 3, pp. 563–567, 1976, doi: 10.1016/0022-1902(76)80305-3.
29. R. J. Atkinson, A. M. Posner, and J. P. Quirk, “Adsorption of potential-determining ions at the ferric oxide-aqueous electrolyte interface,” *Journal of Physical Chemistry*, vol. 71, no. 3, pp. 550–558, Feb. 1967, doi: 10.1021/j100862a014.
30. P. S. Sidhu, “Dissolution of Iron Oxides and Oxyhydroxides in Hydrochloric and Perchloric Acids,” *Clays and Clay Minerals*, vol. 29, no. 4, pp. 269–276, 1981, doi: 10.1346/CCMN.1981.0290404.
31. B. Zhang et al., “Unmasking chloride attack on the passive film of metals,” *Nature Communications*, vol. 9, no. 1, p. 2559, Jul. 2018, doi: 10.1038/s41467-018-04942-x.
32. L. Truche et al., “Experimental reduction of aqueous sulphate by hydrogen under hydrothermal conditions: Implication for the nuclear waste storage,” *Geochimica et Cosmochimica Acta*, vol. 73, no. 16, pp. 4824–4835, Aug. 2009, doi: 10.1016/j.gca.2009.05.043.
33. R. G. Bates and G. D. Pinching, “Acidic dissociation constant of ammonium ion at 0 to 50 °C, and the base strength of ammonia,” *J. Res. Natl. Bur. Stan*., vol. 42, no. 5, p. 419, May 1949, doi: 10.6028/jres.042.037.
34. R. G. Bates and G. D. Pinching, “Acidic dissociation constant and related thermodynamic quantities for monoethanolammonium ion in water from 0° to 50 °C,” *J. Res. Natl. Bur. Stan.*, vol. 46, no. 5, p. 349, May 1951, doi: 10.6028/jres.046.039.
35. G. Olofsson, “Thermodynamic quantities for the dissociation of the ammonium ion and for the ionization of aqueous ammonia over a wide temperature range,” *The Journal of Chemical Thermodynamics*, vol. 7, no. 6, pp. 507–514, Jun. 1975, doi: 10.1016/0021-9614(75)90183-4.
36. S. Ma’mun et al., “Experimental determination of monoethanolamine protonation constant and its temperature dependency,” *MATEC Web Conference.*, vol. 101, p. 02001, 2017, doi: 10.1051/matecconf/201710102001.
37. M. H. Moayed and R. C. Newman, “Deterioration in critical pitting temperature of 904L stainless steel by addition of sulfate ions,” *Corrosion Science*, vol. 48, no. 11, pp. 3513–3530, Nov. 2006, doi: 10.1016/j.corsci.2006.02.010.
38. I. L. Rosenfeld and I. S. Danilov, “Electrochemical aspects of pitting corrosion,” *Corrosion Science*, vol. 7, no. 3, pp. 129–142, Jan. 1967, doi: 10.1016/S0010-938X(67)80073-8.
39. H. P. Leckie and H. H. Uhlig, “Environmental Factors Affecting the Critical Potential for Pitting in 18–8 Stainless Steel,” *Journal of the Electrochemical Society.*, vol. 113, no. 12, p. 1262, 1966, doi: 10.1149/1.2423801.
40. N. Aouina et al., “Initiation and growth of a single pit on 316L stainless steel: Influence of SO_4^{2-} and ClO_4^- anions,” *Electrochimica Acta*, vol. 104, pp. 274–281, Aug. 2013, doi: 10.1016/j.electacta.2013.04.109.
41. T. Hong and M. Naumo, “The Effect of SO_4^{2-} Concentration in NaCl Solution on the Early Stages of Pitting Corrosion of Type 430 Stainless Steel,” *Corrosion Science*, vol. 39, no. 5, pp. 961–967, 1997, doi: 10.1016/S0010-938X(97)81161-4.

42. E. A. Abd El Meguid, N. A. Mahmoud, and S. S. Abd El Rehim, “The effect of some sulphur compounds on the pitting corrosion of type 304 stainless steel,” *Materials Chemistry and Physics*, vol. 63, no. 1, pp. 67–74, Feb. 2000, doi: 10.1016/S0254-0584(99)00206-0.